Langmuir
Article
pubs.acs.org/Langmuir

Fabrication of Nanotubules and Microspheres from the Self-Assembly of Amphiphilic Monochain Stearic Acid Derivatives

Lidong Zhang,[†] Haiqing Li,[†] Chang Sik Ha,[†] Hongsuk Suh,[‡] and Il Kim*,[†]

[†]*The WCU Centre for Synthetic Polymer Bioconjugate Hybrid Materials, Department of Polymer Science and Engineering and* [‡]*Department of Chemistry and Chemistry Institute for Functional Materials, Pusan National University, Pusan 609-735, Korea*

Received July 2, 2010. Revised Manuscript Received October 4, 2010

A series of amphiphilic monochain derivatives of stearic acid, $CH_3(CH_2)_{16}CONH(CH_2)_nNH_2$ (n = 2, 3, 4, 6), $CH_3(CH_2)_{16}CONH(CH_2)_2S_2(CH_2)_2NH_2$, and $[CH_3(CH_2)_{16}CONH]_2(CH_2)_2$, are synthesized, and their self-assembly behaviors have been investigated in 1,2-dichloroethane (DCE). In addition to the concentration of the compound in DCE, the number of methylene units in hydrophilic segments play a crucial role in determining the final morphology of self-assembling structures from nanotubules with 20 nm inner diameter to microspheres with an average diameter of 20 μm. The external texture of the microsphere is also influenced by the number of methylene units in the hydrophilic segment. The microspheres formed by highly ordered aggregattion of nanobelts show high thermal stability. The particular processes and causations have been expatiated.

Introduction

Supramolecular nano- or microinerratic structures coming from the self-assembly of low-molecular-mass monochain derivatives has attracted much interest because of their potential applications in materials science and supramolecular chemistry, involving nanomaterials[1−4] and delivery or modification agents for drugs.[5−8] In general, those monochain derivatives can self-assemble into aggregates of various morphologies, such as belts,[1] tubes,[9,10] ribbons,[11,12] and fibers[13] through hydrogen bonding, $\pi-\pi$ stacking, van der Waals interaction, coordination interaction, and other weak interactions. Some attempts have been made to correlate the properties of the structures of supramolecular nano- or microinerratic structure. Nevertheless, to date, in contrast with large numbers of reports on morphologies such as ribbon and fibers forming from the self-assembly of low-molecular-mass monochain derivatives, spherical structures with mesoporous surface for the more effective applications of delivery or modification agents for drugs have been investigated very little. To the fabrication of tubular structure with greatly simple monochain molecules, some similar works have been reported by previous researchers;[14,15] however, it is still attractive to continue this study more deeply with simple monochain molecules because of some ambiguous issues for the formation of nanotubular structure, such as the control of dimension of tubular structure, concentration effect, and achievement on the monodispersity of nanotubules for diversified molecular structures.

The design and synthesis of novel morphology structure has been an important starting point because nanoscale size, shape, and morphology determine the properties of self-assembled supramolecular structure from the monochain derivatives. The hierarchical self-assembly of nanoscale building blocks can lead to the formation of complex supramolecular assemblies.[16−18]

Inspired by the reported results, we have synthesized a series of low-molecular-weight monochain derivatives of stearic acid. Although lots of compounds derived from stearic acid have been synthesized, especially for various commercial applications,[19−22] to the best of our knowledge, the low-molecular-mass monochain derivatives of stearic acid forming hollow microspheres and nanotubules are not reported. It is well feasible that the chiral monochain derivatives with a diacetylenic segment and a secondary amine salt headgroups could self-assemble to form uniform nanotubules in dichloromethane and hexane.[23,24] However, fabrication and synthesis of new nanotubules and microspheres from achiral center and nondiacetylenic segment in monochain derivatives of low molecular mass are still a significant challenge in supramolecular chemistry.

*To whom correspondence should be addressed. E-mail: ilkim@pusan.ac.kr. Tel: +82-51-510-2466. Fax: +82-51-513-7720.

(1) Cui, H. G.; Muraoka, T.; Cheetham, A. G.; Stupp, S. I. *Nano Lett*. **2009**, *9*, 945.
(2) Hartgerink, J. D.; Beniash, E.; Stupp, S. I. *Science* **2001**, *294*, 1684.
(3) Xiong, Y.; Liu, Q. Y.; Wang, H.; Yang, Y. J. *J. Colloid Interface Sci*. **2008**, *318*, 496.
(4) Sato, I.; Kadowaki, K.; Urabe, H.; Jung, J. H.; Ono, Y.; Shinkai, S.; Soai, K. *Tetrahedron Lett*. **2003**, *44*, 721.
(5) Kang, L.; Liu, X. Y.; Sawant, P. D.; Ho, P. C.; Chanc, Y. W.; Chan, S. Y. *J. Controlled Release* **2005**, *106*, 88.
(6) Sangeetha, N. M.; Maitra, U. *Chem. Soc. Rev*. **2005**, *34*, 821.
(7) Brady, S. F.; Clardy, J. *Org. Lett*. **2005**, *7*, 3613.
(8) Brian, G. F.; Karen, S. L.; Corina, E. R. *Chem. Res*. **2004**, *37*, 421.
(9) Kameta, N.; Masuda, M.; Minamikawa, H.; Goutev, N. V.; Rim, J. A.; Jung, J. H.; Shimizu, T. *Adv. Mater*. **2005**, *17*, 2732.
(10) Kamiya, S.; Minamikawa, H.; Jung, J. H.; Yang, B.; Masuda, M.; Shimizu, T. *Langmuir* **2005**, *21*, 743.
(11) Bhattacharya, S.; Yamuna, K. G. *Chem. Commun*. **2001**, 185.
(12) Spector, M. S.; Singh, A.; Messersmith, P. B.; Schnur, J. M. *Nano Lett*. **2001**, *1*, 375.
(13) Suzuki, M.; Yumoto, M.; Shirai, H.; Hanabusa, K. *Chem.—Eur. J*. **2008**, *14*, 2133.
(14) John, G.; Jung, J. H.; Minamikawa, H.; Yoshida, K.; Shimizu, T. *Chem.—Eur. J*. **2002**, *8*, 23.
(15) Shimizu, T.; Masuda, M.; Minamikawa, H. *Chem. Rev*. **2005**, *105*, 1401.
(16) Sackmann, E. *Science* **1996**, *271*, 43.
(17) Li, L. S.; Stupp, S. I. *Macromolecules* **1997**, *30*, 5313.
(18) Stupp, S. I.; Son, S.; Lin, H. C.; Li, L. S. *Science* **1993**, *259*, 59.
(19) Zhan, C. I.; Gao, P.; Liu, M. H. *Chem. Commun*. **2005**, 462.
(20) Becerril, J.; Burguete, M. I.; Escuder, B.; Luis, S. V.; Miravet, J. F.; Querol, M. *Chem. Commun*. **2002**, 738.
(21) Salmi, C.; Loncle, C.; Vidal, N.; Letourneux, Y.; Brunel, J. M. *Eur. J. Med. Chem*. **2008**, *43*, 540.
(22) Benner, K.; Granzhan, A.; Ihmels, H.; Viola, G. *Eur. J. Org. Chem*. **2007**, *28*, 4721.
(23) Lee, S. B.; Koepsel, R. R.; Russell, A. J. *Nano Lett*. **2005**, *5*, 2202.
(24) Lee, S. B.; Koepsel, R.; Stolz, D. B.; Warriner, H. E.; Russell, A. J. *J. Am. Chem. Soc*. **2004**, *126*, 13400.

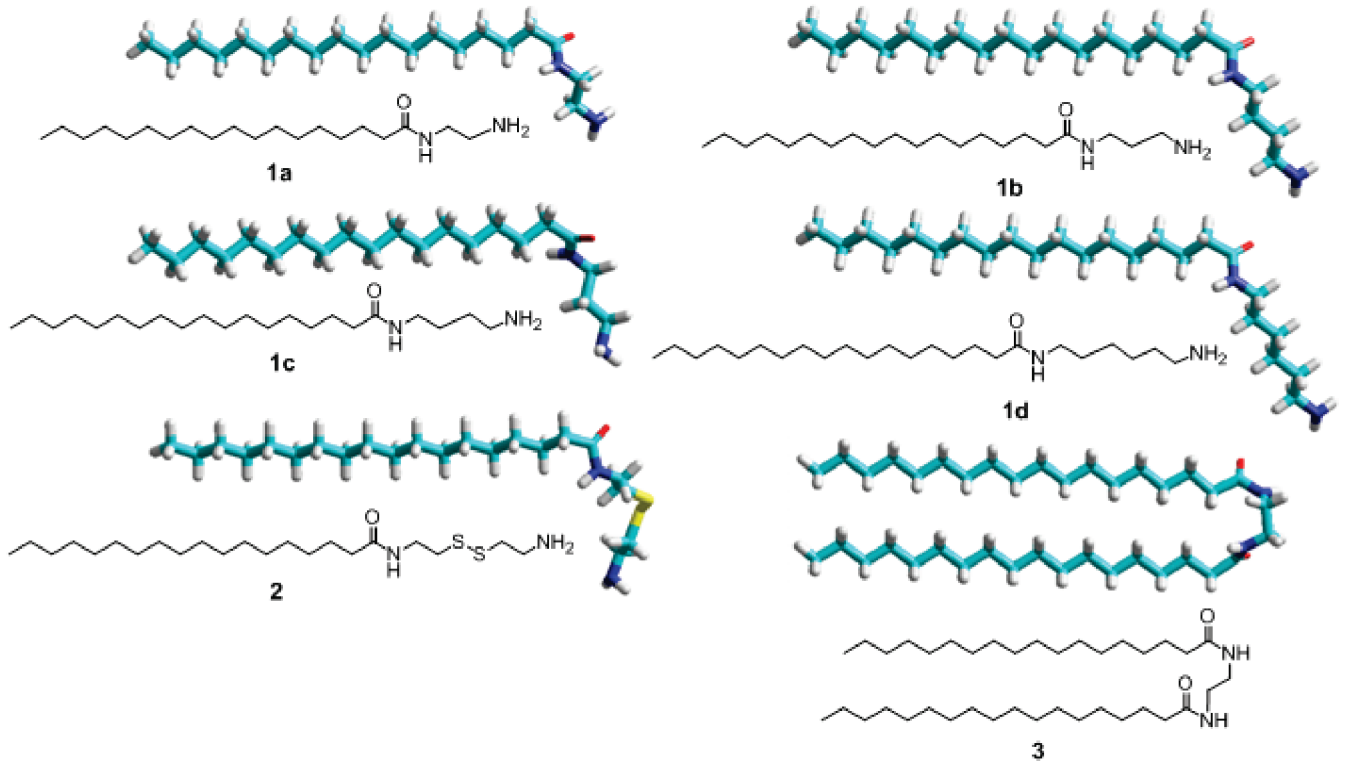

Figure 1. Molecular structures of stearic acid derivatives and their geometry-optimized structures by employing energy minimization algorithm to locate stable structures. The Polak−Ribiere approach in Hyperchem version 8.0 was utilized for calculation.

In this Article, we have focused on the nanotubules and microspheres fabrications based on the self-assembling behavior of amphiphilic derivatives. To search the proper solvents, a series of organic or inorganic solvent and their mixtures has been attempted. The results reveal that 1,2-dichloroethane (DCE) is the optimal organic phase for the formation of nanotubule via a process of thermocooling cycle. It is of great surprise that the number of methylene units in the hydrophilic segment of monochain derivatives is a decisive factor to determine the morphological structure. The effect of the modification of hydrophilic moiety and alkyl chain on the self-assembling behavior is expatiated, and a plausible mechanism has been proposed for the formation of nanotubules and microspheres.

Experimental Details

Materials. Stearic acid (95%), thionyl chloride (99%), pyridine (99.5%), ethylenediamine (99%), 1,3-diaminopropane (99%), cystamine dihydrochloride, 1,4-diaminobutane (99%), hexamethylenediamine (99%), metal sodium, hydrogen tetrachloroaurate trihydrate ($HAuCl_4 \cdot 3H_2O$), and tetraethoxysilane (TEOS) were obtained from Sigma Aldrich, and all of them were used without further purification. DCE, dimethylformamide (DMF), tetrahydrofuran (THF), toluene, and ethanol were distilled before use.

Synthesis. The monochain derivatives of stearic acid (**1a**−**3** in Figure 1) were synthesized starting from stearoyl chloride prepared by the chlorination of stearic acid with thionyl chloride. For example, for the preparation of *N*-(2-aminoethyl) stearamide (**1a**), 0.6 g (0.01 mol) of ethylenediamine was mixed with 0.79 g (0.01 mol) of pyridine in 10 mL of DMF for 10 min at room temperature. After transferring the mixture to the ice bath, 3.02 g (0.01 mol) of stearoyl chloride dissolved in purified DMF (10 mL) was added dropwise for 60 min so that the temperature of the reaction mixture could not exceed 5 °C. The resulting solution was stirred for 10 h at room temperature and then poured in ice water to remove pyridine salt. The white solid obtained by filtration was washed three times by distilled water and dried under vacuum for 24 h at 50 °C.

***N*-(2-Aminoethyl)stearamide (1a).** Colorless solid; yield 90%. mp 100−101 °C. IR (KBr) 3205, 3085, 2927, 2854, 1647, 1568, 1470, 1250, 1123, 940, 714 cm^{-1}. ^1H NMR (300 MHz, $CDCl_3$) δ 0.73−0.75 (m, 3H), 1.12 (m, 28H), 1.43 (m, 2H), 2.03−2.08 (m, 2H), 2.68−2.72 (m, 2H), 3.18−3.19 (m, 2H). ^{13}C NMR (125 MHz, $CDCl_3$) δ 174.32, 42.12, 41.66, 37.13, 32.15, 29.92, 29.90 29.88, 29.84, 29.72, 29.58, 29.56, 26.03, 22.91, 14.33. Anal. Calcd for $C_{20}H_{42}N_2O$: C, 73.56; H, 12.96; N, 8.58. Found C, 72.62; H, 13.21; N, 8.41. Fab-MS *m*/*z* (%) 327.5 (100) $[M + H]^+$.

***N*-(3-Aminopropyl) stearamide (1b).** Colorless solid; yield 85%. mp 89−91 °C. IR (KBr) 3301, 3096, 2927, 1642, 1576, 1473, 1377, 1310, 1153, 731 cm^{-1}. ^1H NMR (300 MHz, $CDCl_3$) δ 0.78 (m, 3H), 1.18 (m, 28H), 1.50 (m, 2H), 1.78 (m, 2H), 2.06 (m, 2H), 2.55 (m, 2H), 3.24 (m, 2H). ^{13}C NMR (125 MHz, $CDCl_3$) δ 174.55, 37.99, 37.73, 35.81, 32.14, 29.92, 29.88, 29.84, 29.73, 29.58, 29.55, 26.07, 22.91, 14.33. Anal. Calcd for $C_{21}H_{44}N_2O$: C, 74.06; H, 13.02; N, 8.23. Found C, 73.54; H, 13.23; N, 8.15. Fab-MS *m*/*z* (%) 341.3 (100) $[M + H]^+$.

***N*-(4-Aminobutyl) Stearamide (1c).** Colorless solid; yield 95%. mp 150−151 °C. IR (KBr) 3319, 3059, 2922, 2849, 1642, 1540, 1475, 1420, 1268, 1214, 954 cm^{-1}. ^1H NMR (300 MHz, $CDCl_3$) δ 0.73 (m, 3H), 1.21 (m, 28H), 1.50 (m, 6H), 2.16 (m, 2H), 2.58 (m, 2H), 3.18 (m, 2H). ^{13}C NMR (125 MHz, $CDCl_3$) δ 173.52, 39.54, 38.82, 35.54, 29.92, 29.90, 29.88, 29.73, 29.58, 29.55, 27.23, 22.91, 14.01. Anal. Calcd for $C_{22}H_{45}N_2O$: C, 74.51; H, 13.07; N, 7.90. Found C, 73.72; H, 13.38; N, 7.67. Fab-MS *m*/*z* (%) 355.5 (100) $[M + H]^+$.

***N*-(6-Aminohexyl) Stearamide (1d).** Colorless solid; yield 95%. mp 144−145 °C. IR (KBr) 3304, 2920, 2850, 1640, 1540, 1467 cm^{-1}. ^1H NMR (300 MHz, $CDCl_3$) δ 0.76 (m, 3H), 1.11 (m, 32H), 1.48 (m, 4H), 2.16 (m, 2H), 2.56 (m, 2H), 3.18 (m, 2H). ^{13}C NMR (125 MHz, $CDCl_3$) δ 173.86, 42.10, 40.82, 32.15, 30.64, 29.92, 29.58, 29.88, 29.84, 29.73, 29.58, 29.55, 27.77, 26.07, 23.34,

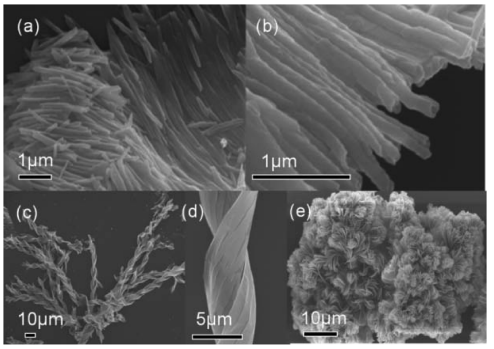

Figure 2. SEM images of the self-assembled structures of compounds **1a** and **3** in 1,2-dichloroethane: (a,b) nanotubule formed from **1a** at low concentration (0.5 mg/mL) and (c,d) twisted breadstick-like (or belt-like) structure from **1a** at high concentration (2.0 mg/mL); (e) chrysanthemum-like microcluster from **3**.

22.91, 14.33. Anal. Calcd for $C_{24}H_{50}N_2O$: C, 75.33; H, 13.17; N, 7.32. Found C, 74.49; H, 13.32; N, 7.19. Fab-MS *m*/*z* (%) 383.6 (100) $[M + H]^+$.

***N*-(2-(2-(2-Aminoethyl) disulfanyl) ethyl) Stearamide (2).** Colorless solid; yield 95%. mp 128−129 °C. IR (KBr) 3319, 2932, 2859, 1643, 1553, 1481 cm^{-1}. ^1H NMR (300 MHz, $CDCl_3$) δ 0.0.75 (m, 3H), 1.21 (m, 28H), 1.50 (m, 2H), 2.16 (m, 2H), 3.40 (m, 2H), 2.85 (m, 2H), 2.60 (s, 4H). ^{13}C NMR (125 MHz, $CDCl_3$) δ 173.45, 40.10, 40.82, 36.15, 36.64, 35.82, 29.92, 29.58, 29.88, 29.84, 29.73, 29.58, 29.55, 27.77, 14.30. Anal. Calcd for $C_{22}H_{45}N_2OS_2$: C, 63.10; H, 11.07; N, 6.69; S, 15.31. Found C, 62.69; H, 11.25; N, 6.61; S, 15.07. Fab-MS *m*/*z* (%) 419.6 (100) $[M + H]^+$.

***N*,*N*′-Ethylenebis (Stearamide) (3).** Colorless solid; yield 95%. mp 150−151 °C. IR (KBr) 3311, 3086, 2921, 2854, 1647, 1570, 1472, 1385, 1251, 1129, 950, 727 cm^{-1}. ^1H NMR (300 MHz, $CDCl_3$) δ 0.75 (m, 6H), 1.12 (m, 56H), 1.42 (m, 4H), 2.04 (m, 4H), 3.26 (m, 4H). ^{13}C NMR (125 MHz, $CDCl_3$) δ 174.21, 41.12, 36.13, 29.92, 29.58, 29.88, 29.84, 29.73, 29.58, 29.55, 27.77, 22.82, 14.21. Anal. Calcd for $C_{38}H_{76}N_2O$: C, 76.96; H, 12.92; N, 4.72. Found C, 76.91; H, 13.01; N, 4.66.Fab-MS *m*/*z* (%) 593.5 (100) $[M + H]^+$.

Self-Assembly Experiments. Compound (2 mg) and DCE (4 mL) were mixed in a sealed test glass tube, and the mixture was then heated in an oil bath until the solution became clear. The resulting solution was cooled slowly to room temperature to precipitate the colorless solid floating in the solvent. Subsequently, the sealed glass test tube was kept under a static condition and then opened to evaporate organic solvent in air.

Characterization. The ^1H NMR spectra of all synthesized compounds were recorded on a Varian Unity Plus (300 MHz) spectrometer, and the fast-atom bombardment (FAB) mass spectra were recorded on a Jeol JMS DX300 apparatus (Jeol, Tokyo, Japan). The surfaces of the self-assembled samples were investigated using a scanning electron microscope (SEM) on a S-4800 apparatus (Hitachi, Japan). A drop of the sample (0.1 mg) dispersed in acetone (1 mL) was applied onto a clean silicon wafer and then slowly dried in air for the SEM observation. The results of self-assembled stearamide derivatives were also characterized by transmission electron microscope (TEM; JEOL 1299EX) operated at 80 keV. Infrared (IR) spectra were measured using a Shimadzu IR Prestige-21 apparatus. X-ray powder diffraction (XRD) patterns of the dried self-assembled powder were measured on a Bruker D8 Focus diffractometer using the Cu Kα radiation. X-ray was generated with a Cu anode, and the Cu Kα beam (λ = 1.5406 Å) was taken out via a graphite monochromator. The long spacing D was obtained from the typical peak. Differential scanning calorimeter (DSC) analysis was performed on a TA Instruments thermal analyzer model DSC 910 under an ultrapure nitrogen atmosphere at a heating rate of 10 °C/min.

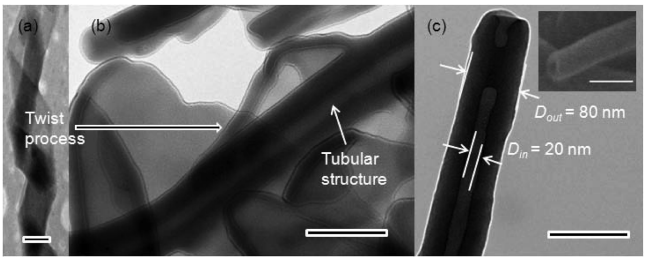

Figure 3. TEM images of the twisted structure coming from **1a** before forming the complete nanotubular morphology (a) and nanotubular structure (b,c). The inset in (c) is an SEM image of the nanotubule. The scale bar in all images is 100 nm.

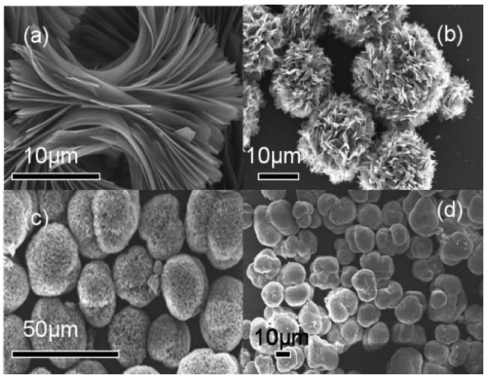

Figure 4. SEM images of the self-assembled structures of compounds **1b**−**d** and **2** in 1,2-dichloroethane: nanobelt-like structure from (a) **1b** and porous microspherical structures from (b) **1c**, (c) **1d**, and (d) **2**.

Results and Discussion

Self-Assembly Behavior. The self-assembly behavior of **1a**−**3** was investigated in various organic solvents, such as ethanol, THF, DMF, chloroform, DCE, and mixed organic−inorganic solvents, such as THF/water, DMF/water, ethanol/water, and so forth. The results revealed that DCE was the best solvent to induce the self-assembly of the monochain derivatives of stearic acid. Figure 2 shows the SEM images of the self-assembled structure of *N*-(2-aminoethyl) stearamide (**1a**) in DCE. The self-assembly was very sensitive to the concentration of **1a**. At a low concentration (0.5 mg/mL), **1a** forms layered nanotubules, confirmed by the SEM in Figure 2a,b, and the TEM in Figure 3b,c, with the inner diameter of ∼20 nm and multilayer wall thickness of ∼30 nm and several micrometers in length. As the concentration increases above 0.5 mg/mL, belt-like nanostructures are formed. As a result, twisted belt-like structures with several tens of micrometers in length, several tens of nanometers in width, and several nanometers in thickness were formed at a concentration of 2.0 mg/mL (Figure 2c,d). Similar structures have been reported for the self-assembly of a peptide amphiphile containing four amino acids and an alkyl tail in water.[1] The formation of nanotubule or twisted nanobelts depending on the concentration of **1a** reveals that the nanotubules deriving from **1a** are of a spiral form or structure coming into being via the self-contortion of nanobelt at low concentration.

The self-assembled morphology was also sensitive to the modification of hydrophilic head groups. Compound **1b** derived from the 1,3-diaminopropane self-assembled to double fan-shaped aggregate morphology, confirmed by SEM in Figure 4a, composed of the belt-like structures ∼100 nm in thickness, 500 nm in width, and several tens of micrometers in length. Under the similar conditions,

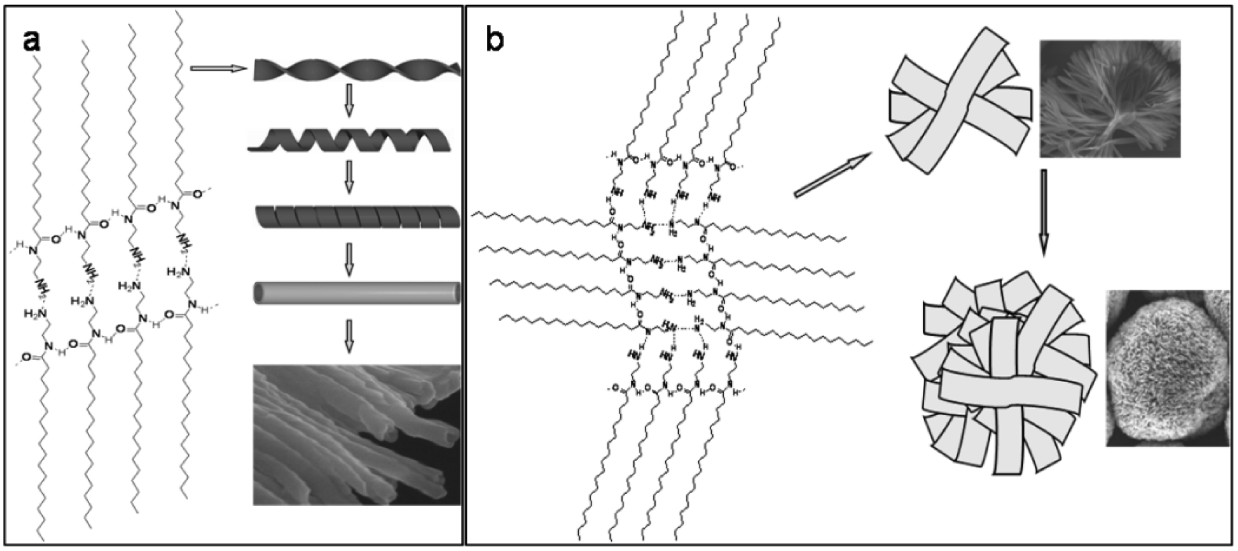

Figure 5. Plausible procedures of the formation of (a) nanotubule and (b) spherical structure by the self-assembly of monochain stearic acid derivatives in 1,2-dichloroethane. The strength and type of hydrogen bond and the concentration of compound play key roles in inducing a specific structure.

1c and **1d** self-assembled to persimmon-like microspheres with the big volume and diameter (Figure 4b,c). The diameters of the microspheres coming from **1c** and **1d** are in the range of 10−20 and 10−30 μm, respectively, and they might be derived from the random aggregate of nonuniform nanobelts. Therefore, the microspheres are in possession of great interspace between nanobelts on the surface and inside. The similar microsphere aggregates could also be generated from compound **2** regardless of the presence of the disulfide groups (Figure 4d). It is interesting to note that the same result is hard to achieve in other solvents such as ethanol, THF, DMF, chloroform, and their mixtures. Our purpose to fabricate compound **2** is to investigate further the effect of the polar headgroup for self-assembly behavior. Using the C−C bond instead of the S−S bond at the polar headgroup should exhibit great transformation on the behavior of the self-assembly. Nevertheless, the tremendous transformation of the self-assembling morphology was not observed from SEM observation in Figure 4. Here we think that the S−S bond has a similar effect as that of the C−C bond for the self-assembly behavior because, as far as the self-assembly is concerned, despite the hydrogen bonding between the S−S and N−H groups, the force of this effect is too weak to change the morphology of self-assembly completely. However, owning to the existence of the weak force, the surface structure of persimmon-like shape formed from the compound **2** becomes closer and smoother, and thus the stability of persimmon-like structure was greatly enhanced. With an increase in chain length from **1c** to **1d** in the hydrophilic fragments, the same transformation with compound **2** on the surface structure of persimmon-like shape can be observed from the SEM observation; these results further proved that the S−S bond plays a similar role as that of the C−C bond for their self-assembly behavior.

To investigate further the effect of hydrophilic headgroup on the self-assembly behavior, we have synthesized double-chain compound **3**, in which the primary amines in ethylenediamine are substituted by stearic acyl groups. The self-assembly was carried out under the similar conditions employed for **1a**. As confirmed by SEM images (Figure 2e), the chrysanthemum-like microclusters coming from the highly ordered aggregation of nanobelts are predominantly observed. The decrease in the concentration of **3** in wide ranges yielded no tubular structure, as observed from the self-assembly of **1a**, demonstrating that the primary amidogen headgroup plays a key role in creating the tubular structure. Besides, the addition of a second tail has greatly increased the hydrophobicity of compound **3** and its critical packing parameter. This can be supported by the result of the modeling of the structure in Figure 1, which clearly shows that the hydrophobe is deeply changed and not only the polar headgroup. The strength to form a head-to-head juncture at the position of the polar part of the compound **3** died down owning to the enhancive steric hindrance and decreased hydrogen bonding effect. However, to compound **1a**, without the steric hindrance existing in the structure, the head-to-head juncture at the position of primary amidogen engenders a long nanobelt shape most probably due to the great hydrogen bonding effect. Subsequently, the resulting long nanobelts would twist themselves layer by layer to produce a nanotubular structure at low concentration. At high concentration, the rolling-up process might be hindered as a result of the steric interaction among a number of neighboring nanobelts.

On the basis of the results mentioned above, a possible mechanism can be proposed for the formation procedure of microspherical and nanotubular structure, as shown in Figure 5. To the nanotubular structure, we observed minor visible twist structures, coexisting with the complete tubular morphologies from the TEM observation, as shown in Figure 3a, and stripe figures on the surface of the nanotubules from the SEM observation in Figure 2b; therefore, we think that the nanobelt morphology was generated in the primary stage because the side hydrogen bonding force existing between N−H and O=C causes the molecule to combine and form a supramolecular belt structure, as shown in Figure 5a, and then twist itself to form a twisted structure due to the concentration effect.[25] In a general way, the belt can easily roll up or twist itself to form a multilayer or monolayer nanotubule via a heating−cooling circulation or solvent evaporation.[14,15] Nevertheless, to extraordinary long nanobelts, the behavior of rolling up will be embarrassed and substituted by twisted self-assembly under the proper concentration condition. Our experimental results indicated that the nanotubular structure experienced a self-twist and not a rolling up procedure.

(25) Chen, Y. L.; Zhu, B.; Zhang, F.; Han, Y.; Bo, Z. S. *Angew. Chem., Int. Ed.* **2008**, *47*, 6015.

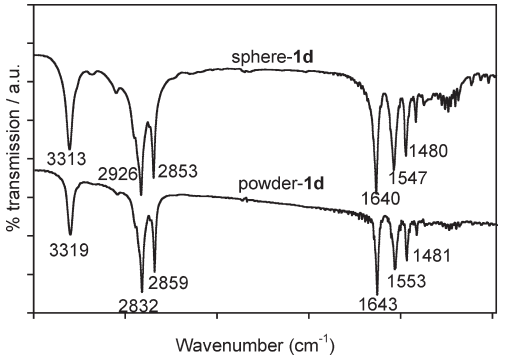

Figure 6. IR spectra of **1d** before (powder) and after (sphere) self-assembly.

To the microspherical structure, with the increase in the number of methylene units of hydrophilic segment, the space at the joint of the head-to-head of the molecule becomes bigger. Therefore, the molecular conjugation also takes place easily at the lateral joint to form a physically cross-linked structure, as shown in Figure 5b, but the probability for the physically cross-linked structure to roll up or twist itself is greatly decreased. Consequently, the one and only manner for its self-assembling behavior is that the highly ordered aggregate, by using the joint point as a core and the alkyl chain as a tail, could be progressed as parallel connecting from both sides of molecule attributing to the strong hydrogen bonding force. The simple process is shown in Figure 5b. The mechanism of generating a microsphere includes three processes: (i) the amphiphilic monomers conjoin each other as the way of head to head at the hydrophilic segment to engender nanobelt morphology, (ii) the twist of nanobelt is occurred only at the joint point, and (iii) the twisted segment acts as a core of persimmon-like microsphere, which is created because of greatly inerratic aggregate behavior.

Spectroscopic Investigation. The FT-IR spectroscopy as a powerful tool for investigating the hydrogen bonding interaction has been proverbially applied in the analysis of the morphology of self-assembling organic compounds. According to the FT-IR spectroscopy, the characteristic IR bands of the compounds **1a**, **1b**, **1c**, **1d**, **2**, and **3** were observed approximately 3309−3320 ($\upsilon_{as}NH_2$, υNHCO), 2930 ($\upsilon_{as}CH_2$), 2851 (δ_sCH_2), 1642 (υC═O), 1545 (υNH, υCN), and 1480 cm^{-1} (δCH_2). However, after assembling to special morphologies the peak signals of diversified group assignments of **1a**, **1b**, **1c**, **1d**, **2**, and **3** show blue shift. As an example, Figure 6 shows FT-IR spectra of **1d** before and after self-assembly, and Table 1 summarizes the results of assignments. All IR signals relating to the formation of hydrogen bonding from the powder sample before self-assembly to self-assembled samples show a red shift, such as N−H and O═C. The peaks at 3319 and 1553 cm^{-1} for the powdery sample that are assigned to NH_2 stretching and υ(N−H), shift to 3313 and 1547 cm^{-1}, respectively, for the self-assembled microspheres. The similar blue shifts have also been observed from the absorption bands of the asymmetric (υ_{as}) and symmetric (υ_s) $-CH_2$ stretching vibrations. As a result, the peaks at 2932 (υ_{as}) and 2859 cm^{-1} (υ_s) of the powdery sample shift to 2926 and 2853 cm^{-1}, respectively, for the self-assembled microsphere. This is because the frequencies of the alkyl chain antisymmetric and symmetric stretching bands are very sensitive to the conformation of the hydrocarbon chain.[26] The absorption bonds were observed at 2926 and 2853 cm^{-1} in the self-assembled microsphere, indicating the presence of an all-trans-zigzag form

(26) Sapper, H.; Cameron, D. G.; Mantsch, H. H. *Can. J. Chem.* **1981**, *59*, 2543.

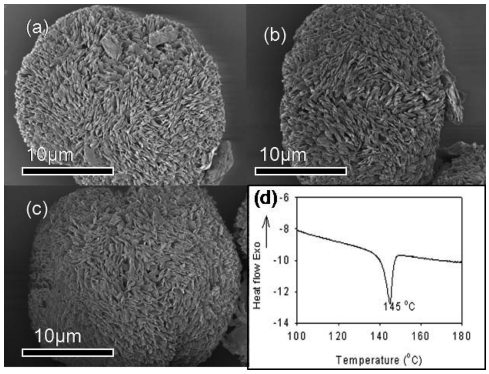

Figure 7. SEM images taken after thermal treatment of the self-assembled microsphere from **1d**: (a) heating at 50 °C for 1 h, (b) heating at 90 °C for 1 h, and (c) heating at 130 °C for 1 h. (d) DSC curve of the self-assembled microsphere from **1d**.

Table 1. FT-IR Band Assignments of 1d before (Powder) and after (Sphere) Self-Assembly

assignments	absorption peak of sample (cm^{-1})	
	self-assembled microsphere	solid powder
$\nu_{as}(NH_2)\nu$(NHCO)	3313	3319
$\nu_{as}(CH_2)$	2926	2932
$\delta_s(CH_2)$	2853	2859
ν(C═O)	1643	1643
ν(NH), ν(CN)	1547	1553
$\delta(CH_2)$	1480	1481

alkyl chain.[27,28] The eigenvalue of the carboxyl group also shifts from 1643 cm^{-1} of the powder to 1640 cm^{-1} of the microsphere. These results testify the existence of strong hydrogen-bonding interactions between O═C and H−N as well as N−H and N−H bonding, which plays critical role in the formation of self-assembled nanobelt and highly ordered microsphere aggregate. The primary amine group in **1d** undergoes a lateral and head-on hydrogen-bonding interaction to form a physically cross-linked structure. Therefore, it becomes clear that the self-assembly of **1d** occurs by means of hydrogen-bonding between the primary-amino/secondary-amino groups and hydrophobic interactions between the alkyl groups, even though van der Waals interaction, coordination interaction, and other weak interactions cannot be completely neglected.

Thermal Stability of Self-Assembled Microsphere. As a means of investigating the stability of the self-assembled structures, the microsphere obtained by **1d** was subject to heat treatment controlled by TA Instruments thermal analyzer model DSC 910 under an ultrapure nitrogen atmosphere at a heating rate of 10 °C/min at different temperatures for 1 h; then, the morphology was retraced. The result, as shown in Figure 7, reveals the thermal stability of the microsphere **1d** in keeping the highly ordered microspherical structure after heating the sample of self-assembled **1d** at different temperature for 1 h separately. The microspheres display expectedly high thermal stability at a wide range of temperature lower than its melting point (145 °C; Figure 7d). For example, as shown in Figure 7, the samples retain their original shapes after heating to 50, 90, and 130 °C for 1 h under nitrogen atmosphere, except that the surface of the samples becomes slightly smooth at 90 and 130 °C. These results demonstrate that the aggregated

(27) Fujimoto, Y.; Ozaki, Y.; Kato, T.; Matsumoto, N.; Iriyama, K. *Chem. Phys. Lett.* **1992**, *196*, 347.
(28) Luo, X. Z.; Li, Z. f.; Xiao, W.; Wang, Q.; Zhong, J. l. *J. Colloid Interface Sci.* **2009**, *336*, 803.

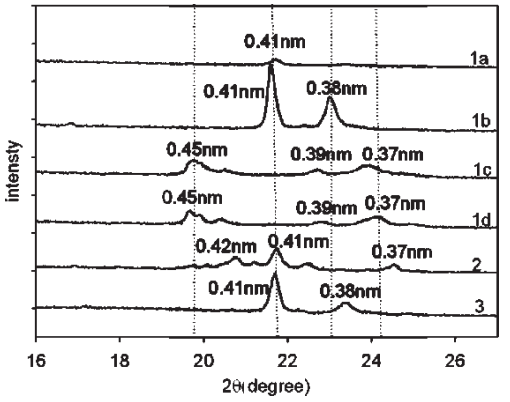

Figure 8. X-ray powder diffraction patterns of self-assembled samples from **1a**, **1b**, **1c**, **1d**, **2**, and **3**.

structures formed by the self-assembled nanobelts show very good thermal stability before melting.

X-ray Diffraction Study. The XRD patterns of the self-assembled powder samples obtained by **1a** to **3** are depicted in Figure 8. The observed single peak with *d* spacing of 0.41 nm for nanotubule coming from the self-assembly of **1a** demonstrates the ordered packing of the alkyl chains, which also proves that the nanotubular structure is characterized by the uniform shape and dimension. The XRD patterns of the self-assembled structures of **1b** and **3** are similar to the *d* spacing of 0.41 and 0.38 nm, respectively. This suggests a greatly ordered nanobelt phase attributing to a repeat unit along the long axis of the molecule.

The position of the XRD peaks shifts greatly with the increase in the number of methylene units in hydrophilic segment, due to transformations of self-assembling structure. The similarity of the peaks observed for the self-assembled structures of the compounds **1c** and **1d** with the *d* spacing of 0.45 and 0.37 nm is caused by their similar microspherical structures. It is interesting to note that the self-assembled powder from **2** shows quite different XRD curves from self-assembled structures from **1c** and **1d** despite the similar textural morphology based on the electron microphotograph. Comparing the XRD curve from **2** with those from **1b** and **3**, the former is characterized by an obvious peak at 21.68° with the *d* spacing of 0.41 nm, illuminating the microspherical structure from **2** that is generated via the highly ordered aggregation of nanobelts. The peaks at 20.73° with the *d* spacing of 0.42 nm and 24.51° with the *d* spacing of 0.37 nm observed from the self-assembled structure from **2** demonstrate that it has more compact surface than that of microspheres from **1c** and **1d**.

Conclusions

The self-assembly of a series of amphiphilic monochain derivatives of stearic acid shows that the concentration of the compound, the type of solvent, and the number of methylene units in the hydrophilic segment play critical roles in determining the final morphology. The self-assembly at low concentration of *N*-(2-aminoethyl)stearamide in DCE yields nanotubules with outer diameter of ~80 nm, whereas twisted belt-like nanostructures are formed at high concentration. By the simple modification of the hydrophilic headgroups, various nano- and microstructures such as nanobelt, porous microspheres, and chrysanthemum-like microclusters are obtained. The formation of spherical structure depends greatly on the effect of steric hindrance in the hydrophilic segment among the stearic derivatives, where the correspondingly large steric helps the nanobelts to twist themselves to bring into being the tubular structure. Additionally, the surface of the microsphere becomes smoother and closer with the augment of the number of methylene units in the hydrophilic segment. The fabrication of microsphere from these simple stearic acid derivatives with low molecular mass and without chiral center has altered various conventional self-assembling structures such as nanofiber, nanoribbon, nanovesicle, and so forth. The high thermal stability of the self-assembled structures can be addressed on the basis of thermal annealing study. The XRD study shows that the uniform shape and dimension of the self-assembled structures are induced by the ordered packing of the alkyl chains.

Acknowledgment. This work was supported by grants-in-aid for the *World Class University Program* (no. *R*32-2008-000-10174-0).

Supporting Information Available: More SEM images of the nanotubules formed by the self-assembly of the compound **1a** at low concentration in DCE. This material is available free of charge via the Internet at http://pubs.acs.org.